J Mater Sci (2020) 55:12747–12760

Ceramics

Hydroflux-assisted densification: applying flux crystal growth techniques to cold sintering

Sarah Lowum[1,*], Richard Floyd[1], and Jon-Paul Maria[1]

[1] *Department of Materials Science and Engineering, The Pennsylvania State University, 215 Steidle Building, University Park, PA 16802, USA*

Received: 6 May 2020
Accepted: 7 June 2020
Published online: 17 June 2020

ABSTRACT

Hydroflux-assisted densification (HAD) is introduced as a method for low-temperature ceramic densification. HAD expands upon the cold sintering process, using an inorganic "hydroflux" secondary mass transport phase as opposed to the aqueous acidic, basic, or salt solutions that have been reported previously. Hydrofluxes combine ionic salts with sparing quantities of water to depress their melting points into the cold sintering range. The substantial solubility of many oxides in these hydrofluxes makes them appealing transport phases for an expanded cold-sinterable materials spectrum. This paper focuses on a hydroflux transport phase containing a eutectic mixture of NaOH and KOH (called "NaK") for which particular nuances and properties are discussed. We demonstrate HAD in the ZnO system, highlighting the importance and impact of processing variables such as pressure, transport phase quantity, and water content. Additionally, we show densification of the oxide binaries Bi_2O_3, WO_3, CuO, and MnO, and the functional ternaries Bi_2WO_6 and $K_xNa_{1-x}NbO_3$ in the 200–300 °C range. This entire set is challenging to cold sinter using aqueous transport phases.

Introduction

Low-temperature ceramic densification has gained growing interest over the past several decades as continuous technological innovations drive demand for improved materials properties and integration. Reducing ceramic sintering temperatures to several hundred Celsius is imperative for co-processing with polymers [1–3], metals [4, 5], or other temperature-sensitive compounds [6, 7]. This low thermal budget also slows or prevents many other undesirable sintering effects, such as coarsening, volatilization, or high-temperature defect chemistries that are retained post-sintering. Roy and Gouda demonstrated dense, high-strength ceramic compacts at temperatures of ~ 250 °C by hot pressing hydrated cements in the 1970s [8, 9]. In 1986, Yamasaki et al. introduced hydrothermal hot pressing, a technique modeled after sedimentary rock lithification [10]. In this process, relatively large volume fractions of water, typically between 10 and 30 wt%, were added

Address correspondence to E-mail: sml92@psu.edu

https://doi.org/10.1007/s10853-020-04926-7

to ceramic powders that were then pressed under hydrothermal conditions up to 350 °C [10–12]. In 2014, the Jantunen Group at Oulu University demonstrated room temperature densification of Li_2MoO_4 by adding 2–3 wt% of water and applying 130 MPa of pressure in a conventional pellet die [13].

Two years later, the Randall Group at Penn State University expanded on low-temperature densification work and introduced the "Cold Sintering Process" in which they combined a ceramic powder, a secondary aqueous mass transport phase, and moderate pressure to facilitate densification in a wide variety of materials systems at temperatures 300 °C or below [14]. The mass transport phases used in cold sintering have primarily been water or aqueous solutions of acids, salts, or bases [3]. Only a few cases have been reported in which other organic solvents were used, primarily to avoid unwanted secondary phases originating from water-driven reactions [7, 15, 16]. Water is a common trend among all of these low-temperature densification methods, further summarized in Grasso et al. [17].

Conversely, recent work by Floyd et al. illustrated that ZnO can be cold-sintered to 97% dense using only $Zn(OAc)_2•2H_2O$, with no liquid water, as a mass transport phase [18]. Sinterometry, an automated cold sintering method providing in situ compaction analysis, enabled this discovery [19]. This observation raises questions regarding the role of water and liquids during cold sintering and suggests opportunities to implement a broader set of secondary transport phases, including salts that are solid at room temperature. However, similar experiments attempting to use hydrated acetates to cold sinter Bi_2O_3 and NiO, two materials systems that had proven challenging to densify with aqueous acetate or acetic acid solutions, were not as successful [20]. Collectively, these observations revealed a new class of mass transport phases for cold sintering: inorganic, flux-based solvents.

Since ionic salts are commonly used for crystal growth, it seemed only appropriate to seek inspiration from flux-based techniques. Flux crystal growth uses a high-temperature melt of an inorganic compound as the solvent for crystallization. Initially, this posed a challenge since most fluxes are effective only at temperatures above 300 °C [21], which is outside the cold sintering temperature regime. However, in their 1975 book Elwell and Scheel discussed the possibility of a "hydroflux" method for growing oxide crystals [22]. This technique combined flux crystal growth and hydrothermal growth by using water to modify the properties, notably melting point, of molten salt fluxes. Elwell and Scheel stated molten salts containing up to 50 mol% water could act as hydrofluxes [22]. William Chance, a doctoral student in the zur Loye group at the University of South Carolina, conducted his dissertation work on crystal growth using hydrofluxes [23]. Chance defined hydrofluxes as belonging to a compositional regime where melts have high water contents, but the water remains solvated in the melt, as opposed to an aqueous solution where the flux is solvated in the water [24]. This prevents high pressures like those generated during hydrothermal growth. Additionally, water suppresses the flux melting temperatures, enabling use in the low temperatures required by cold sintering.

In this paper, we report using hydrofluxes as mass transport phases during cold sintering in a method termed hydroflux-assisted densification (HAD) [25]. Specifically, a eutectic 51:49 mol% mixture of NaOH:KOH was selected as the preliminary flux composition to test and will be the focus of this paper as initial proof of concept for HAD. This flux mixture, referred to as "NaK," was selected given its conveniently low eutectic melting point of 170 °C and the noted high solubility of many oxides in hydroxides [26]. Furthermore, this melting point is likely easily suppressed by small quantities of water, following the hydroflux concept, making this transport phase an ideal candidate for low-temperature ceramic densification.

Experimental

Powder processing and preparation

Bi_2WO_6 was synthesized via solid-state reaction. Bi_2O_3 (Alfa Aesar, 12230, 99%, calcined at 650 °C for 4 h) and WO_3 (Sigma-Aldrich, 95410, 99.9%) were mixed in a stoichiometric ratio, ball-milled in ethanol for 24 h, then dried in an 80 °C vacuum oven (~ 0.2 atm) to evaporate the ethanol. The Bi_2O_3-WO_3 mixture was heated to 700 °C at 10 °C/min and held for 4 h. The resulting Bi_2WO_6 powder was ball-milled in methanol for 48 h. Commercial MnO (Sigma-Aldrich, 377201, 99%), WO_3 (Sigma-Aldrich, 95410, 99.9%), and CuO (Alfa Aesar, 12299, 97%) powders

were ball-milled in methanol for 24 h, and ZnO powder (Alfa Aesar, 44263, 99.9%) was ball-milled in methanol for 48 h to breakup agglomerates and aggregates. Milled powders were dried in a rotary evaporator to remove the methanol. Bi_2O_3 powder (Alfa Aesar, 12230, 99%) and $K_xNa_{1-x}NbO_3$ powder (PI Ceramics) were not milled. All powders were dried for 2 days in an 80 °C vacuum oven (~ 0.2 atm) and then stored in a glovebox purged with dry air (< 10 ppm H_2O).

Commercial NaOH (Millipore, SX0590-1, A.C.S. Grade) and KOH (Fisher Scientific, P250-500, A.C.S. Grade) pellets were obtained for the transport phase. The hydroxides were mixed with the ceramic powders in two forms: an aqueous solution and a powder. To form the aqueous solutions, 30 wt% NaOH or KOH was dissolved in DI water. The solutions were then added to the ceramic powder by weight via a hypodermic needle. It should be noted that this process was carried out in an ambient laboratory environment with fluctuating humidity, as will be discussed later. The ceramic-transport phase formulation was mixed in a FlackTek SpeedMixer™ (Model DAC 150.1 FVZ) and subsequently dried in an 80 °C vacuum oven (~ 0.2 atm) until the liquid water was removed (10–30 min, depending on the amount of added solution), leaving behind the uniformly dispersed NaK transport phase.

To form the hydroxide powders, the starting hydroxide pellets were dissolved in DI water and the solution was then dried in an 80 °C vacuum oven (~ 0.2 atm) until all liquid water evaporated and the hydroxides precipitated into finer crystallites. The hydroxide precipitates were subsequently crushed in the SpeedMixer™ using cylindrical YSZ milling media to form fine hydroxide powders, dried again in an 80 °C vacuum oven (~ 0.2 atm), and then stored in a dry glovebox. The glovebox was purged with dry air (< 10 ppm H_2O) in addition to being connected to a DRI-TRAIN HE-493 recirculation system designed to remove moisture, allowing it to maintain a relative humidity less than 1%. Given the hygroscopic nature of NaOH and KOH, HAD formulations using the powdered hydroxides were stored and weighed in the dry glovebox environment to better control moisture content. A hypodermic needle was used to add small quantities of water to powder mixtures in certain circumstances. The combined parent powder-transport phase mixture was then sealed in a plastic FlackTek SpeedMixer™ cup and removed from the glovebox. Mixing was conducted in the SpeedMixer™ such that the transport phase could be uniformly distributed among the ceramic powder without opening the sealed container and exposing the mixture to the ambient laboratory environment, minimizing water absorption or evaporation to negligible levels. The only point in which the powder formulations were exposed to the ambient laboratory environment was in the final step of loading the pellet die; however, the total exposure time was generally less than 10 s. Experiments quantifying the change in moisture content of powder formulations with respect to time (discussed in the Results and discussion section) revealed that in 10 s there is negligible water absorption or evaporation. Discussion on the benefits and disadvantages of incorporating the hydroxide transport phase as an aqueous solution vs. a powder is included in the Results and discussion section.

Custom-built equipment for hydroflux-assisted densification

Preliminary experiments with the NaK transport phase were conducted in 440C stainless steel pellet dies, commonly used for cold sintering [3]; however, the higher temperatures (200–300 °C vs 120 °C) and more aggressive transport phase (i.e., concentrated hydroxide) led to severe die erosion after only a few samples. An erosion track developed on the interior die wall at the position of the ceramic powder mixture, causing pellets to crack and break on extraction. To address this die erosion issue, a custom-built tungsten carbide pellet die was used for further HAD experiments with the NaK transport phase. This die consisted of a tungsten carbide drill bushing, supported by an outer stainless-steel shaft collar, and tungsten carbide punches. The die was heated by a Tempco Mi-plus 400 W heater band at a maximum ramp rate around 55 °C/min and temperature was monitored by a thermocouple placed into a hole drilled in the shaft collar. Temperature was controlled with a Tempco TEC-8450 controller. Prior to any experiments, a temperature calibration was performed by placing a second thermocouple on the interior die wall and measuring the difference between the outer thermocouple reading and the actual temperature inside the die. This difference ranged from 5 to 20 °C, depending on the set temperature, and was due to the slight mismatch in

thermal expansion between steel and WC, leading to temperature-dependent thermal contact between the bushing and shaft collar. Figure 1a, b shows a disassembled and assembled WC die, respectively. This die proved far more resilient against extreme temperatures (up to 300 °C), pressures (up to 1.4 GPa), and corrosive environments and was likewise named the "armadillo die." A sheet of filter paper was used between the ceramic powder and the die punches during experiments to further help maintain punch face integrity. Post-densification and pre-characterization, sample surfaces were roughly polished with sandpaper.

Samples were pressed in the armadillo die at pressures ranging from 90 to 530 MPa using the sinterometer, an automatic hydraulic press designed and built by the Maria group specifically for in situ monitoring of low-temperature densification processes [19]. This instrument includes a linear displacement sensor that tracks compaction as a function of time during densification experiments, ultimately providing the opportunity to plot sintegrams—compaction traces of densification experiments that are corrected to account for die thermal expansion. These sintegrams provide information similar to that obtained from a dilatometer or calorimeter; however, data can be collected under the unique pressure and temperature conditions exhibited in HAD and cold sintering. More details about sinterometer design and function are described in Floyd et al. [19].

Characterization

Sample densities were measured both volumetrically and by the Archimedes method. Measured densities were compared against theoretical values (ZnO—5.61 g/cm^3, MnO—5.37 g/cm^3, WO_3—7.16 g/cm^3, CuO—6.31 g/cm^3, Bi_2O_3—8.90 g/cm^3, Bi_2WO_6—9.5 g/cm^3, $K_xNa_{1-x}NbO_3$—4.7 g/cm^3) to calculate relative density. X-ray diffraction (XRD—Panalytical Empyrean) was used to investigate sample crystallinity and phase purity. Scanning electron microscopy (VP-FESEM—Zeiss Sigma) was employed to study fracture surface microstructure.

Results and discussion

Nuances of the NaK transport phase

As discussed in the Experimental section, the NaK transport phase was added to the ceramic starting powder both as an aqueous solution and as a dry powder. The justification behind each approach stems from two obstacles posed by this new "solid" transport phase: (1) It is challenging to uniformly disperse small quantities of secondary hydroxide powder among a parent ceramic powder in the absence of a liquid and (2) early experiments revealed that small quantities of water can dramatically alter the densification process when using hydroxide transport phases. In light of these observances, experiments were conducted employing both approaches to better examine the NaK transport phase behavior and appreciate the nuances.

Initial experiments used the aqueous hydroxide solutions because this method was perceived as superior for evenly dispersing the NaOH and KOH, originally in the form of large pellets, among the ceramic particles. However, when adding the hydroxides as a solution then drying the powder to remove the water, it is easy to generate ZnO samples with significant variations in final density and microstructure (Fig. 2), despite being processed with the same parameters (transport phase quantity, pressure, temperature, time). These density and microstructural differences appear to be related to

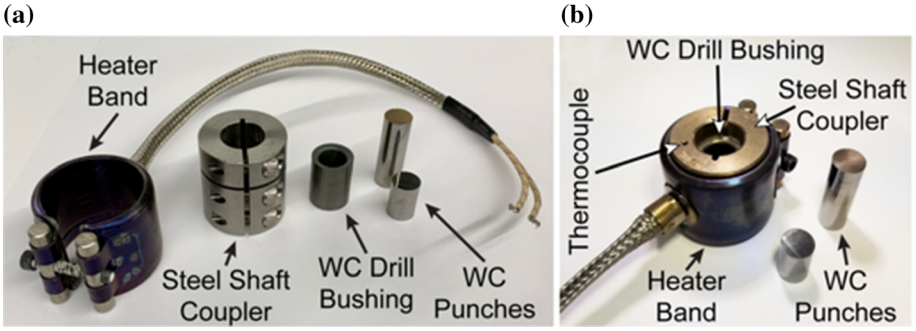

Figure 1 Images showing **a** a disassembled and **b** assembled WC "armadillo" die that was used for hydroflux-assisted densification experiments described in this paper.

small changes in water content of the powder formulation, induced by variations in drying or large day-to-day swings in ambient laboratory humidity.

Such humidity effects are mentioned in a previous paper by Floyd et al. discussing the impact of the ambient humidity of the powder storage environment on final density of ZnO samples cold-sintered with a solid $Zn(OAc)_2 \bullet 2H_2O$ transport phase. Floyd et al. show that sample density peaks when powders are stored at 55% RH [18]. Given that both acetates and hydroxides are aggressively hygroscopic compounds, changes in ambient processing humidity can cause significant changes in water content of these transport phases. Chance et al. reported that commercial hydroxides often contain around 15 wt% water, which changes melting point and solvent properties [24]. Similar humidity effects were not previously seen in most cold sintering experiments using aqueous solutions, likely due to the fact that these solutions contributed an excess of water to the process that was then lost via evaporation or extrusion out of the die [27]. However, a few studies have reported enhanced compaction/densification in powders stored in humid environments [28, 29]. With non-aqueous, inorganic transport phases, such as hydrated metal acetate powders or NaK, small quantities of water play a critical role in the densification process.

Following the inconsistencies experienced when adding the NaK via aqueous solution, a new approach was taken: adding the hydroxides in a powder form and weighing/combining the ceramic powders and transport phase in a dry (< 1% RH) glovebox environment. This method posed its own challenges, primarily difficulties in even distribution of the hydroxide powders among the ceramic parent powder. However, the use of the dry glovebox and hydroxide powders made possible the study of the impact of water on the HAD technique using the NaK transport phase, in addition to improving experimental reproducibility. Given the proven dependence on water content and the nonequilibrium state of HAD (i.e., high pressures in a semi-sealed system), baseline experiments were conducted to investigate the properties of the NaK transport phase itself.

The first experiment investigated the interaction between NaK and the ambient laboratory atmosphere, specifically looking at water absorption and desorption with varying ambient humidities. 1.000 g of ZnO was mixed with 15 vol% and 5 vol% of the "dry," powdered NaK in the glovebox. This mixture was then exposed to the ambient laboratory environment at 55% RH, and the water absorption over time was measured via mass gain. The results are plotted in Fig. 3a. The powder mixed with 15 vol% NaK absorbed water at an average rate of 0.6 mg/min (0.06 wt%/min), while the powder mixed with 5 vol% NaK absorbed water at an average rate of 0.3 mg/min (0.03 wt%/min). Although this may seem like an inconsequential amount, many early experiments revealed that small quantities of water on the order of a few milligrams could result in density changes > 10%. This experiment also indicates that the powder–environment interaction depends on transport phase quantity.

A second similar experiment was conducted to measure the rate of water evaporation in the glovebox. This experiment was used to verify that water would not evaporate at a rate faster than it can be added. A SpeedMixer™ cup containing 30 mg of

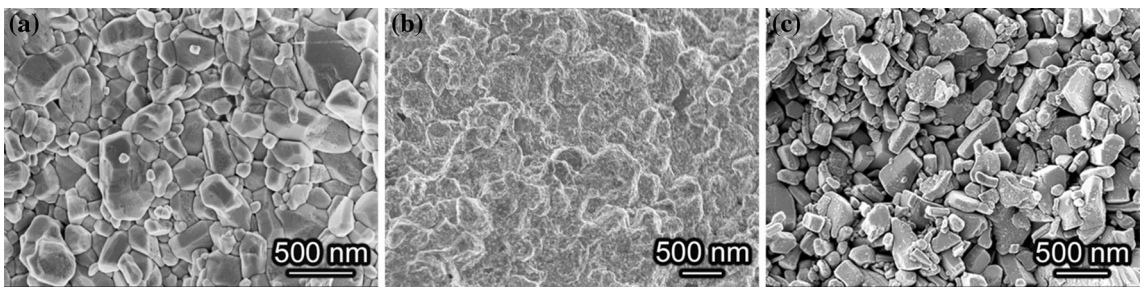

Figure 2 SEM images of fracture surfaces of three different ZnO samples all cold-sintered with 3 vol% NaK, at 530 MPa and 200 °C for 30 min. Despite being cold-sintered under the same conditions, the three samples have drastically different densities and microstructures: **a** 97% dense with a clean, low porosity microstructure and clearly formed grain boundaries, **b** 98% dense with a large quantity of secondary phase in the microstructure, **c** 75% dense with a clean, high-porosity microstructure and minimal changes in grain morphology compared to the starting powder (see Fig. 6a).

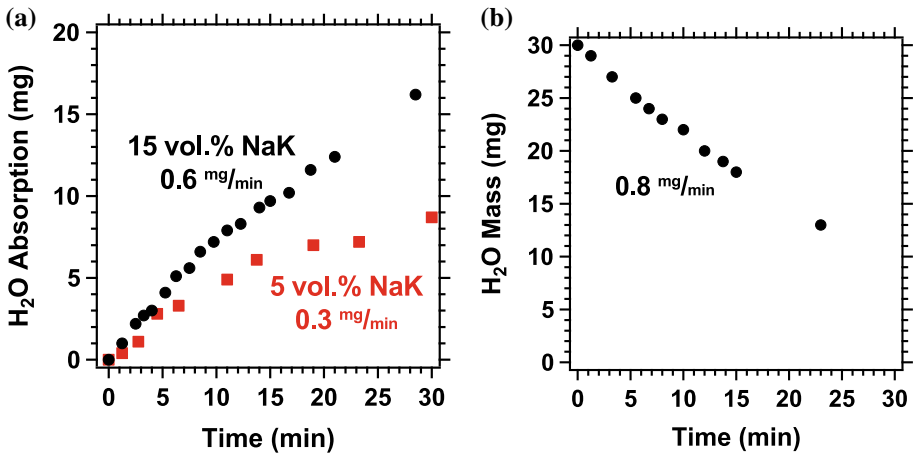

Figure 3 **a** The rate of water absorption of a mixture of 1.000 g of dry ZnO with varying volume fractions of dry NaK exposed to 55% RH and **b** the rate of water evaporation in the dry (< 1% RH) glovebox environment.

water (quantities added to powder formulations are typically < 30 mg) was exposed to the dry (< 1% RH) air in the glovebox, and mass loss was recorded with time. An evaporation rate of 0.8 mg/min was recorded, as seen in Fig. 3b. This experiment represented a worst-case scenario, as mixing the water with the powder slows the evaporation rate to about 0.2 mg/min. When mixing powder formulations in the glovebox, water is added last and the SpeedMixer™ cup is capped within 15 s, so minimal water will evaporate during this time.

Additionally, the melting behavior of the 51:49 NaOH:KOH mixture was investigated using the sinterometer. It is known from the literature absorbed water can lower the melting point of hydroxides [24]. However, the high pressures (~ 100 s of MPa) applied during HAD likely favor the solid phase of the hydroxides, given that NaOH and KOH have higher molar volumes in the liquid phase [30, 31]. Figure 4a shows a plot of compaction vs. time of NaK under a pressure of 530 MPa. The compaction event beginning at ~ 13 min is attributed to melting of the NaK mixture. This is concluded based on the large amount of compaction (~ 0.8 mm) and observations of material being extruded out of the top and bottom of the die at this point in the experiment. It should be noted that for this experiment the die ramp rate was slowed to 10 °C/min to more easily identify the melting onset temperature. Figure 4b plots compaction rate, as determined by taking the differential with respect to time of the trace in (a), after smoothing (for clarity). Examining the differential sintegram in Fig. 4(b), the NaK mixture melted between 148 and 158 °C, which is slightly lower than the 170 °C eutectic melting point predicted by the phase diagram. This is most likely attributed to absorbed water suppressing the melting point [24].

Densification trends in the ZnO-NaK system

The impact of general HAD variables, including water quantity, pressure, temperature, transport phase quantity, and time, was studied using ZnO and NaK as a model system. All experiments presented for this system were prepared in the dry glovebox using the powdered NaK. The first set of experiments focused on water quantity. ZnO was mixed with 2 and 5 vol% NaK and pressed at 90 MPa and 200 °C for 30 min, while water content was varied from 0 to 20 vol%. It is important to note "0 vol%" indicates that no water was added to the sample; however, it is difficult to say how much adsorbed water remained on the surface of the powder in the glovebox. Water readily adsorbs to the ZnO surface and forms a particularly stable monolayer structure often consisting of molecular water and dissociated hydroxyls [32–34]. Experimental work by Meyer et al. using helium thermal desorption spectroscopy (He-TDS) showed the maximum desorption peak for water on the ZnO surface occurred around 100 °C [32]; however, other experimental and computational work has shown that it can take temperatures greater than 300 °C or a vacuum of 10^{-5} Torr to remove all physisorbed and chemisorbed water from the ZnO surface [33–35]. If one assumes 100 nm cubic grains, then a monolayer coating of water equates to ~ 0.2 vol%.

The relatively low pressure (90 MPa) used in this experimental set is also worth pointing out. Much of the prior cold sintering work conducted by the Maria

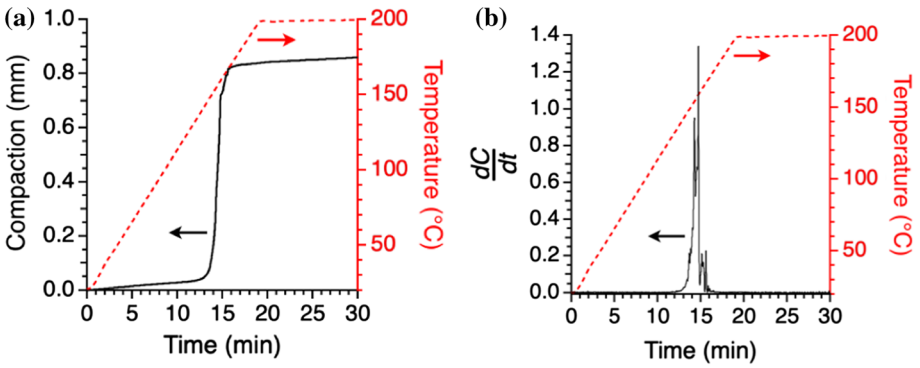

Figure 4 A plot of **a** compaction vs. time for pure, dry NaK (stored in a glovebox at < 1% RH) pressed at 530 MPa and **b** the differential with respect to time of the compaction trace in **a** showing changes in compaction rate that indicate the onset of melting of the NaK. The compaction trace in **a** was smoothed prior to differentiating to reduce noise in the differential trace. Based on **b**, melting of the NaK occurs between 148 and 158 °C.

group was performed at pressures near 500 MPa; however, for such low-temperature densification techniques to become widely adopted in industry and scaled-up, the necessary pressure must be reduced to a more achievable value. Hence, experiments were conducted at low pressure to see whether the HAD approach could be beneficial for reducing densification pressures. As shown in Fig. 5, at a 2% volume fraction of NaK no samples achieve a density above 70%, regardless of water content. However, for a 5% volume fraction of NaK there is a clear peak in density (96% theoretical) at 5 vol% water, suggesting a critical water fraction needed to support and complete the sintering process, and a threshold above which additional amounts impede densification. This hindered densification was seen in cold-sintered NaCl as well, where adding water decreased final sample density because the water became trapped in the sample, leaving behind pores once it evaporated [36]. This effect could also be related to the transition between a "hydroflux," or a flux with solvated water, and an aqueous solution, water with a solvated flux. As mentioned previously, aqueous solutions generate significant hydrostatic pressure in the die due to the water expanding, which could limit densification at low applied pressures [27].

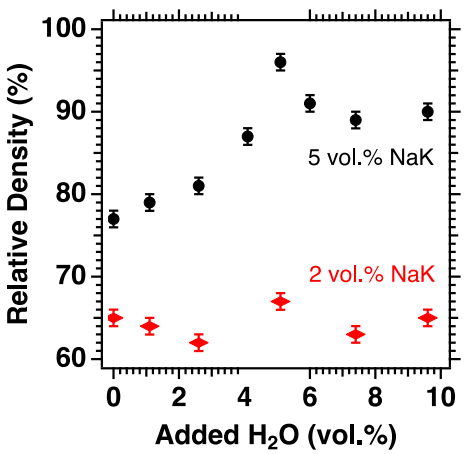

Figure 5 Relative density as a function of volume fraction of added H_2O for ZnO samples prepared in the glovebox and cold-sintered with 2 and 5 vol% NaK at 90 MPa and 200 °C for 30 min.

Microstructures of samples densified with 0, 5, and 10 vol% added H_2O (Fig. 6) reveal that even the sample with 0 vol% added H_2O (Fig. 6b) shows clear changes in grain morphology and microstructure from the starting powder (Fig. 6a). Grains appear more equiaxed in the post-HAD sample when compared to the more anisotropic, prismatic particles found in the starting powder. Additionally, grain boundary formation is visible in the post-HAD sample. Although high density was not achieved in the sample with 0 vol% added H_2O, these results indicate that HAD may be activated by small water quantities, such as those associated with residual physisorbed or chemisorbed water after drying. ReaxFF simulations presented by Sengul et al. revealed that water can aid in cold sintering ZnO with acetic acid solutions by reducing the adsorption energy for Zn^{2+} on the ZnO surface, by promoting a vacancy-rich surface that improves surface diffusion, and also by activating a separate water-mediated surface diffusion mechanism that mimics diffusion rates typically only achieved at high temperatures [37]. Other studies have reported that adsorbed water can aid or even hinder sintering of oxide ceramics by

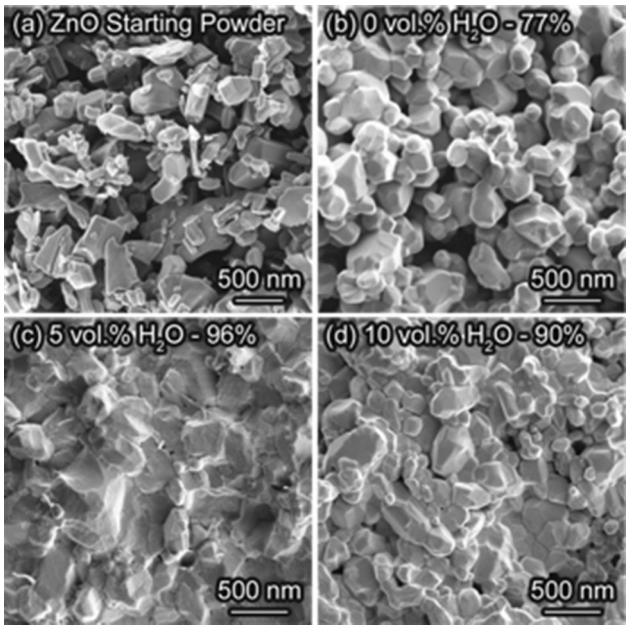

Figure 6 **a** ZnO starting powder (post-milling) and microstructures of ZnO samples cold-sintered with 5 vol% NaK at 90 MPa and 200 °C for 30 min with **b** 0 vol% added H_2O, **c** 5 vol% added H_2O, and **d** 10 vol% added H_2O. Relative densities are included on the micrographs.

influencing surface diffusion processes [38–41]. Water may be playing a key role in the surface adsorption and diffusion processes proceeding during HAD, leading to the peak in the data presented in Fig. 5.

Additionally, water could potentially suppress the flux melting temperature [24] or promote uniform mixing and distribution of the flux among the powder particles. As depicted in Fig. 7, which visually compares a ZnO sample densified with NaK and no added water to one densified with 5 vol% added water, water addition clearly aids the in transport phase distribution among the ceramic powder. The sample with no added water appears splotchy, while the sample with added water appears more uniform in color. At this time, the fundamental role of water in the HAD process is not clear; however, this will be further investigated in future work. Though, it is important to note that the NaK transport phase allows for high-density samples at low pressures (90 MPa), pending the ideal amount of added water.

Densification trends as a function of pressure were also investigated. Previous work has shown that cold sintering with aqueous-based transport phases requires hydrothermal-like conditions to achieve full

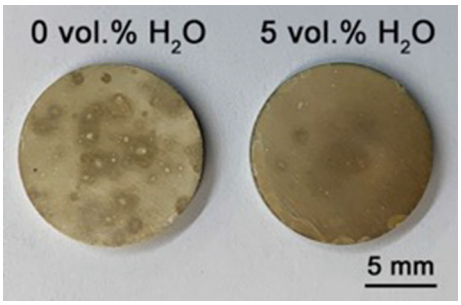

Figure 7 Comparison of a sample densified with 2 vol% powdered NaK and no added water (left) and a sample densified with 2 vol% powdered NaK and 5 vol% added water (right). The addition of water appears to help in distributing the transport phase among the ceramic powder, as evidenced by the improved uniformity in color of the sample with added H_2O.

density [27]. Therefore, plotting relative density vs. pressure revealed an abrupt jump in density around a critical pressure value, which was correlated to the uniaxial applied pressure needed to counteract the hydrostatic pressure generated as the water expands on heating [27]. It was hypothesized that hydroflux-assisted densification may show a different pressure trend given that water content has been drastically reduced. Operating in the "hydroflux" regime also assumes subcritical hydrothermal conditions and overall lower pressures generated within the die [24]. An experiment with the ZnO-NaK system was conducted where pressure was varied between 35 and 530 MPa, while other variables were held constant (2 vol% NaK, 200 °C, 30 min). Two sample sets were collected: one for samples with no added H_2O and one for samples with 5 vol% added H_2O. As seen in Fig. 8, the resulting density–pressure trend shows a smooth, gradual increase in density with increasing pressure. A "critical" pressure value is not seen, unlike in the ZnO-aqueous $Zn(OAc)_2$ system [27], but the trend is similar to that of the ZnO-$Zn(OAc)_2$•2-H_2O system presented in Floyd et al. [18]. There does not appear to be any distinct differences in trend for the samples with 0 vol% added H_2O compared to those with 5 vol% H_2O. It is clear that pressure can compensate for reduced transport phase quantities, since samples with 2 vol% NaK reached 97% dense at 530 MPa, whereas it took 5 vol% NaK to achieve the same density at 90 MPa. Additionally, dense samples prepared by the HAD technique using NaK do not seem to form any notable secondary phases by X-ray diffraction, regardless of water content, as presented in Fig. 9.

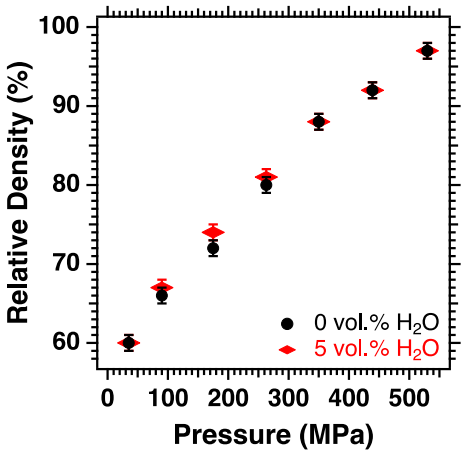

Figure 8 Relative density as a function of pressure for ZnO samples prepared in the glovebox with 2 vol% NaK and 0 or 5 vol% added H_2O and then cold-sintered at 200 °C for 30 min. It should be noted the samples pressed at 35 MPa were pressed in a manual Carver Model M press, as the sinterometer experiences instability at such low pressures.

Application of HAD to other material systems

The NaK transport phase has expanded the set of materials that can be cold-sintered beyond ZnO. Table 1 presents a compilation of binary oxide materials densified with NaK, including HAD parameters and final densities, while Fig. 10 shows representative microstructures of fracture surfaces. The samples described by Table 1 and Fig. 10 were densified with NaK added via the aqueous solution approach. Initial successes were seen with this solution method; however, attempts to cold sinter many of these materials using the powdered NaK were inconsistent and often did not result in as high densities. This is believed to be primarily a mixing issue. As previously mentioned, it is challenging to uniformly distribute small quantities of secondary NaOH and KOH powder among the ceramic powder in a dry environment. Appreciable densification did still occur in the powdered NaK case and changes in grain morphology were clearly visible when examining samples through SEM, further indicating that the slightly lower densities of the dry-processed samples may be related to transport phase distribution. This is a challenge that needs to be addressed in future work.

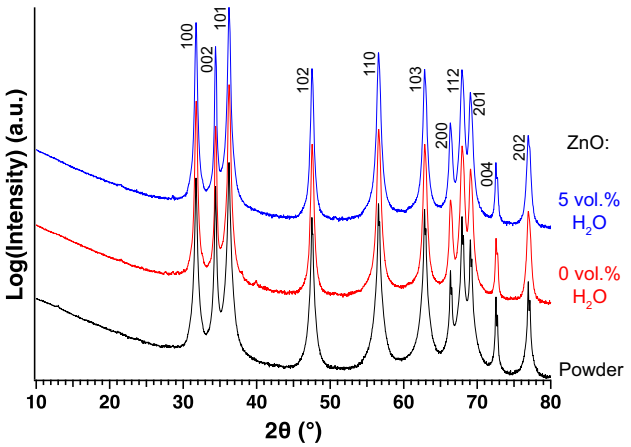

Figure 9 X-ray diffraction patterns for ZnO starting powder (bottom), ZnO cold-sintered at 530 MPa and 200 °C with 2 vol% NaK and 0 vol% H_2O (middle), and ZnO cold-sintered at 530 MPa and 200 °C with 2 vol% NaK and 5 vol% H_2O (top). ZnO remains the primary phase fraction post-HAD with NaK, with negligible secondary phase formation in either sample.

Several materials listed in Table 1 had previously proven difficult to cold sinter with aqueous-based solutions. Early attempts to densify CuO with acidic aqueous solutions showed no signs of densification, indicated by the lack of mechanical rigidity of the sample and the minimal change in particle morphology [42]. Applying the HAD technique, CuO was densified to 93% at 200 °C and 95% at 300 °C. Figure 11, an XRD comparison of the CuO starting powder, CuO densified at 200 °C, and CuO densified at 300 °C, demonstrates an important point, however. Although one may be inclined to push temperatures higher to ease densification of troublesome materials, this can lead to notable secondary phase formation, which may be detrimental to properties. For CuO densified at 200 °C, some small peaks, likely related to sodium and potassium carbonate phases, are present in the diffraction pattern; however, the primary phase fraction remains CuO. Though, raising the densification temperature to 300 °C results in significant formation of Cu_2O and Cu metal, which was easily visible on the sample surface given its distinct color. This ultimately results in a composite material, rather than the phase-pure oxide starting material. One must remain mindful of this as these low-temperature densification techniques are continually expanded to new materials.

This new class of transport phases opens a window of opportunities for low-temperature densification that previously seemed out of reach. In addition to the binary oxides listed in Table 1, the NaK transport phase has already demonstrated success in densifying functional ternary materials. This work explored

Table 1 Assortment of binary oxides that have been successfully densified by the HAD technique at temperatures of 300 °C or below. Densification conditions, final densities, and any secondary phases formed during the HAD process (see Fig. 11 and Figures S1–S3 in the electronic supplementary material for XRD plots) are included. All densities are relative to the primary oxide phase

Material	Vol% NaK	Temp. (°C)	Relative density (%)	Secondary phases
Bi_2O_3	10	200	95	–
WO_3	7	200	92	$W_2O_6(H_2O)$
CuO	5	200	93	$KHCO_3$ (minor), γ-Na_2CO_3 (minor)
CuO	5	300	95	Cu_2O, Cu, β-Na_2CO_3
MnO	5	200	94	Mn_3O_4, $Mn(OH)_2$, $Na_2C_2O_4$, K_4CO_4

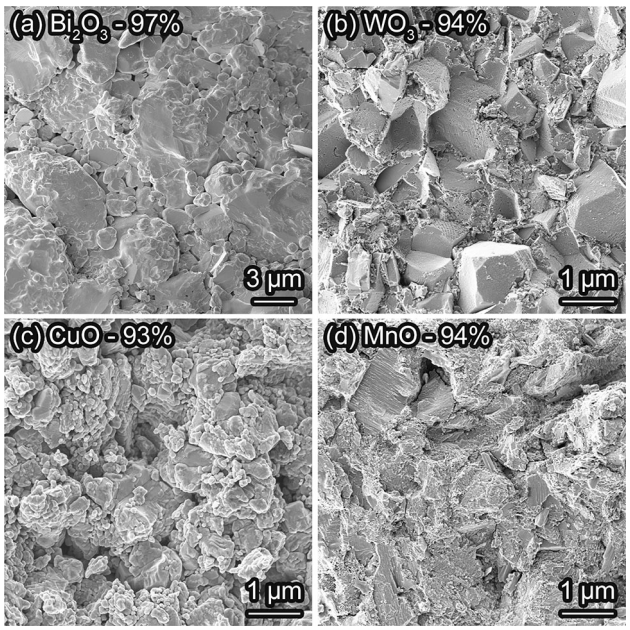

Figure 10 Representative microstructures of **a** Bi_2O_3 + 10 vol% NaK, **b** WO_3 + 7 vol% NaK, **c** CuO + 5 vol% NaK, and **d** MnO + 5 vol% NaK all cold-sintered at 530 MPa and 200 °C for 30 min. Relative densities are included on the micrographs, and SEM images of starting powders are included in Figure S4 in the electronic supplementary material.

HAD of Bi_2WO_6, given that Bi and W cations had proven amenable to this densification approach, and $K_xNa_{1-x}NbO_3$, due to the presence of Na and K in the parent ceramic. Preliminary densification attempts resulted in 88% dense Bi_2WO_6 and 94% dense $K_xNa_{1-x}NbO_3$. Representative microstructures are presented in Fig. 12 for each material. Examining the micrograph of Bi_2WO_6 in Fig. 12a, the lack of porosity would indicate a density much higher than 88%. X-ray diffraction revealed notable quantities of secondary Bi_2O_3 and $K_3Na(WO_4)_2$ phases were present in the densified ceramic (Figure S5 in the electronic supplementary material), which could have been related to secondary bismuth tungstate phases of varying stoichiometry present in the starting powder. Based on a refinement of the diffraction pattern for the densified sample, it was estimated to contain ~ 30% Bi_2O_3 and ~ 10% $K_3Na(WO_4)_2$. Applying a rule of mixtures to estimate a new theoretical density would result in a relative density closer to 95%, which aligns more closely with the dense microstructure. $K_xNa_{1-x}NbO_3$ did not appear to form any secondary phases following the HAD process (Figure S6 in the electronic supplementary material).

Both Bi_2WO_6 and $K_xNa_{1-x}NbO_3$ are materials of interest for their ferroelectric and piezoelectric properties. $K_xNa_{1-x}NbO_3$ in particular has been targeted as a lead-free replacement for PZT; however, it presents major challenges during sintering due to Na and K volatility leading to changes in stoichiometry at high temperatures [43]. HAD offers a potential route to achieve dense samples at low temperatures, avoiding volatility issues and stoichiometry changes. Furthermore, the low temperatures used in HAD provide unique opportunities to carefully tailor microstructure and study the microstructural impacts on functional properties. The ferroelectric grain size effect has piqued the interest of ceramists for many years; however, it is challenging to conduct a controlled study that alters grain size while keeping other processing conditions constant. The HAD technique could help address this problem. The Randall Group at Penn State has already started to explore this possibility in the classic ferroelectric, $BaTiO_3$. They successfully densified $BaTiO_3$ to densities > 90% while maintaining grain sizes under 200 nm [44]. Previous attempts to cold sinter $BaTiO_3$ with aqueous transport phases required post-processing heat treatments between 700 and 900 °C to achieve useful properties [45], but the HAD approach eliminated the need for these secondary heat treatments. One could

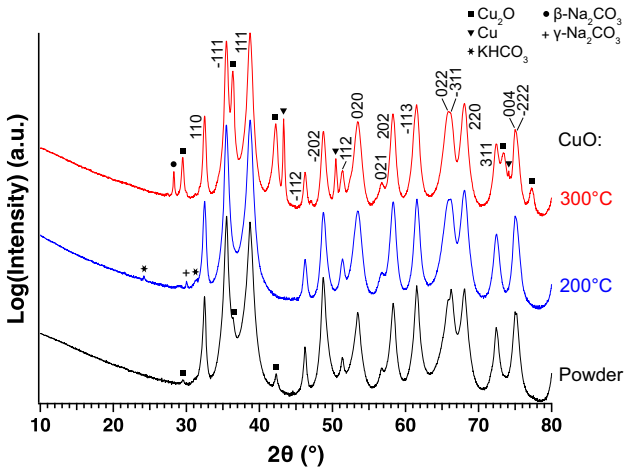

Figure 11 XRD traces of CuO starting powder (bottom), CuO densified with 5 vol% NaK and 530 MPa for 30 min at 200 °C (middle) and 300 °C (top). Increasing the temperature from 200 to 300 °C results in significant secondary phase formation of Cu_2O and Cu metal.

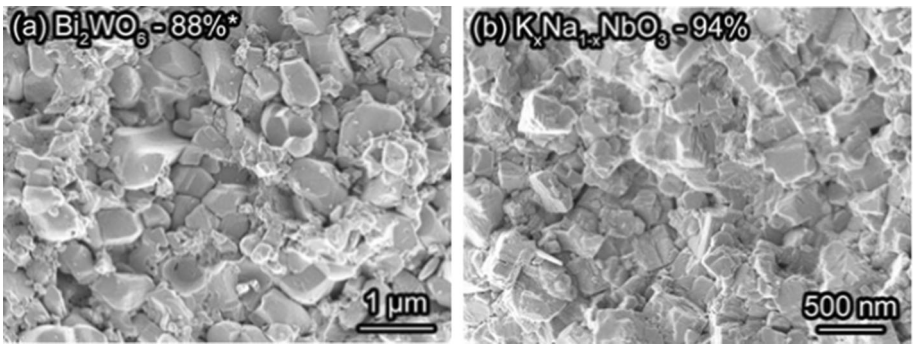

Figure 12 Functional ternary materials densified using the HAD technique. **a** Bi_2WO_6 densified with 10 vol% NaK at 530 MPa and 200 °C for 30 min and **b** $K_xNa_{1-x}NbO_3$ densified with 5 vol% NaK at 530 MPa and 300 °C for 30 min. Final relative densities (as compared to the parent material) are included on the micrographs. *Bi_2WO_6 formed approximately 30% Bi_2O_3 and 10% $K_3Na(WO_4)_2$ (based on refinement of the XRD pattern), making the estimated relative density closer to 95%. SEM images of starting powders are included in Figure S4 in the electronic supplementary material.

imagine a variety of other applications where enabling low-temperature densification would lead to interesting applications to advance both scientific understanding and employable technology.

The data presented above for binary oxides and ternary materials only represent preliminary attempts to apply the NaK transport phase to a wide variety of ceramics and do not depict ideal conditions. As illustrated by the data presented for the ZnO-NaK system, there is a large space for optimization by understanding the impact of the many processing parameters involved in the HAD technique (water quantity, pressure, temperature, time, etc.). The primary goal of this initial work is to establish that these new inorganic "hydroflux" transport phases show great promise in expanding the spectrum of materials amenable to low-temperature densification.

Conclusions

Hydroflux-assisted densification (HAD) is a derivative of the cold sintering process focusing on inorganic, flux-based transport phases and significantly reduced water quantities. Using a 51:49 mol% ratio of NaOH:KOH (NaK) as the transport phase, it was shown that a variety of binary oxides as well as functional ternary materials (Bi_2WO_6 and $K_xNa_{1-x}NbO_3$) could be densified at temperatures of 300 °C or

below. When studying densification in the ZnO-NaK system, it was seen that all processing parameters (transport phase quantity, water quantity, pressure, temperature, and time) play a critical role in the HAD process. Strategically altering these variables can even allow for high-density samples at a relatively low pressure of 90 MPa. This indicates that there is a large space for optimization of the HAD process providing hope that this process may be valuable for densifying more complex materials with functional properties. However, the details are critical in expanding this technique to such materials, as small changes in experimental variables have proven able to significantly alter results. Therefore, a deeper understanding of the role of each processing variable in the densification process and the interactions between each will be crucial for densifying functional materials with tailorable properties.

Acknowledgements

The authors acknowledge Professor Paul Maggard of North Carolina State University for his helpful suggestions to draw comparisons between cold sintering processes and flux crystal growth processes. The authors would also like to thank members of the Huck Institutes of the Life Sciences' Microscopy and Cytometry Facility at the Pennsylvania State University for use of their equipment. This material is based upon work supported by the National Science Foundation, as part of the Center for Dielectrics and Piezoelectrics under Grant Nos. IIP-1841453 and IIP-1841466. This material is based upon work supported by the National Science Foundation Graduate Research Fellowship Program under Grant No. DGE1255832. Any opinions, findings, and conclusions or recommendations expressed in this material are those of the author(s) and do not necessarily reflect the views of the National Science Foundation.

Compliance with ethical standards

Conflict of interest The authors are unaware of any conflicts of interest regarding the data and findings presented in this manuscript.

Electronic supplementary material: The online version of this article (https://doi.org/10.1007/s10853-020-04926-7) contains supplementary material, which is available to authorized users.

References

[1] Guo J, Berbano SS, Guo H, Baker AL, Lanagan MT, Randall CA (2016) Cold sintering process of composites: bridging the processing temperature gap of ceramic and polymer materials. Adv Funct Mater 26:7115–7121

[2] Zhao X, Guo J, Wang K, Herisson De Beauvoir T, Li B, Randall CA (2018) Introducing a ZnO–PTFE (polymer) nanocomposite varistor via the cold sintering process. Adv Eng Mater 20:1–8

[3] Maria JP, Kang X, Floyd RD, Dickey EC et al (2017) Cold sintering: current status and prospects. J Mater Res 32:3205–3218

[4] Baker A, Guo H, Guo J, Randall C, Green DJ (2016) Utilizing the cold sintering process for flexible-printable electroceramic device fabrication. J Am Ceram Soc 99:3202–3204

[5] Guo J, Baker AL, Guo H, Lanagan M, Randall CA (2017) Cold sintering process: a new era for ceramic packaging and microwave device development. J Am Ceram Soc 100:669–677

[6] Xie Y, Yin S, Yamane H, Hashimoto T, Sato T (2009) Low temperature sintering and color of a new compound $Sn_{1.24}Ti_{1.94}O_{3.66}(OH)_{1.50}F_{1.42}$. Solid State Sci 11:1703–1708

[7] Berbano SS, Guo J, Guo H, Lanagan MT, Randall CA (2017) Cold sintering process of $Li_{1.5}Al_{0.5}Ge_{1.5}(PO_4)_3$ solid electrolyte. J Am Ceram Soc 100:2123–2135

[8] Roy DM, Gouda GR (1973) High strength generation in cement pastes. Cem Concr Res 3:807–820

[9] Gouda GR, Roy DM (1976) Characterization of hot-pressed cement pastes. J Am Ceram Soc 59:412–414

[10] Yamasaki N, Yanagisawa K, Nishioka M, Kanahara S (1986) A hydrothermal hot-pressing method: apparatus and application. J Mater Sci Lett 5:355–356

[11] Anagisawa K, Sasaki M, Nishioka M, Ioku K, Yamasaki N (1994) Preparation of sintered compacts of anatase by hydrothermal hot-pressing. J Mater Sci Lett 13:765–766

[12] Hosoi K, Hashida T, Takahashi H, Yamasaki N, Korenaga T (1997) Solidification behaviour of calcium carbonate via aragonite-calcite wet transformation with hydrothermal hot pressing. J Mater Sci Lett 16:382–385

[13] Kähäri H, Teirikangas M, Juuti J, Jantunen H (2014) Dielectric properties of lithium molybdate ceramic fabricated at room temperature. J Am Ceram Soc 97:3378–3379

[14] Guo J, Guo H, Baker AL, Lanagan MT, Kupp ER, Messing GL, Randall CA (2016) Cold sintering: a paradigm shift for

processing and integration of ceramics. Angew Chemie Int Ed 55:11457–11461

[15] Kang X, Floyd R, Lowum S, Long D, Dickey E, Maria JP (2019) Cold sintering with dimethyl sulfoxide solutions for metal oxides. J Mater Sci 54:7438–7446

[16] Bin HW, Li L, Yan H, Chen XM (2019) Cold sintering and microwave dielectric properties of dense HBO_2-II ceramics. J Am Ceram Soc 102:5934–5940

[17] Grasso S, Biesuz M, Zoli L, Taveri G et al (2020) A review of cold sintering processes. Adv Appl Ceram 119:115–143

[18] Floyd RD, Lowum S, and Maria J-P (2020) Cold sintering zinc oxide with a crystalline zinc acetate dihydrate mass transport phase. Submitted for publication.

[19] Floyd R, Lowum S, Maria J-P (2019) Instrumentation for automated and quantitative low temperature compaction and sintering. Rev Sci Instrum 90:055104

[20] Floyd RD (2019) Improving the instrumentation and science of cold sintering. PhD Dissertation, North Carolina State University

[21] Bugaris DE, Zur Loye HC (2012) Materials discovery by flux crystal growth: quaternary and higher order oxides. Angew Chemie 51:3780–3811

[22] Elwell D, Scheel HJ (1975) Crystal growth from high-temperature solutions. Academic Press Inc., London

[23] Chance MW (2014) Hydroflux synthesis: a new and effective technique for exploratory crystal growth. PhD Dissertation, University of South Carolina

[24] Chance WM, Bugaris DE, Sefat AS, Zur Loye HC (2013) Crystal growth of new hexahydroxometallates using a hydroflux. Inorg Chem 52:11723–11733

[25] Maria J-P, Floyd RD, and Lowum S (2019) Hydroflux-assisted densification. US Patent U.S. Provisional Patent Application.

[26] Mugavero SJ, Gemmill WR, Roof IP, Zur Loye HC (2009) Materials discovery by crystal growth: lanthanide metal containing oxides of the platinum group metals (Ru, Os, Ir, Rh, Pd, Pt) from molten alkali metal hydroxides. J Solid State Chem 182:1950–1963

[27] Kang X, Floyd R, Lowum S, Cabral M, Dickey E, Maria JP (2019) Mechanism studies of hydrothermal cold sintering of zinc oxide at near room temperature. J Am Ceram Soc 102:4459–4469

[28] Dargatz B, Gonzalez-Julian J, Guillon O (2015) Improved compaction of ZnO nano-powder triggered by the presence of acetate and its effect on sintering. Sci Technol Adv Mater 16:25008

[29] Gonzalez-Julian J, Neuhaus K, Bernemann M, Pereira da Silva J, Laptev A, Bram M, Guillon O (2018) Unveiling the mechanisms of cold sintering of ZnO at 250°C by varying applied stress and characterizing grain boundaries by Kelvin Probe Force Microscopy. Acta Mater 144:116–128

[30] Dauby C, Glibert J, Claes P (1979) Electrical conductivity and specific mass of the molten NaOH-KOH eutectic mixture. Electrochim Acta 24:35–39

[31] Janz GJ (1967) Molten Salts Handbook, 1st edn. Academic Press Inc., New York, NY

[32] Meyer B, Marx D, Dulub O, Diebold U, Kunat M, Langenberg D, Wöll C (2004) Partial dissociation of water leads to stable superstructures on the surface of zinc oxide. Angew Chemie Int Ed 43:6641–6645

[33] Wöll C (2007) The chemistry and physics of zinc oxide surfaces. Prog Surf Sci 82:55–120

[34] Raymand D, van Duin ACT, Spångberg D, Goddard WA, Hermansson K (2010) Water adsorption on stepped ZnO surfaces from MD simulation. Surf Sci 604:741–752

[35] Morimoto T, Nagao M, Tokuda F (1968) Desorbability of chemisorbed water on metal oxide surfaces. I. Desorption temperature of chemisorbed water on hematite, rutile, and zinc oxide. Bull Chem Soc Jpn 41:1533–1537

[36] Li L, Bin HW, Yang S, Yan H, Chen XM (2019) Effects of water content during cold sintering process of NaCl ceramics. J Alloys Compd 787:352–357

[37] Sengul MY, Guo J, Randall CA, van Duin ACT (2019) Water-mediated surface diffusion mechanism enables the cold sintering process: a combined computational and experimental study. Angew Chemie 131:12550–12554

[38] Varela JA, Whittemore OJ, Longo E (1990) Pore size evolution during sintering of ceramic oxides. Ceram Int 16:177–189

[39] Anderson PJ, Morgan PL (1964) Effects of water vapour on sintering of MgO. Trans Faraday Soc 60:930–937

[40] Angle JP, Morgan PED, Mecartney ML (2013) Water vapor-enhanced diffusion in alumina. J Am Ceram Soc 96:3372–3374

[41] Dargatz B, Gonzalez-Julian J, Bram M, Jakes P et al (2016) FAST/SPS sintering of nanocrystalline zinc oxide-Part I: enhanced densification and formation of hydrogen-related defects in presence of adsorbed water. J Eur Ceram Soc 36:1207–1220

[42] Kang X (2017) Hydrothermal cold sintering. PhD Dissertation, North Carolina State University

[43] Zhen Y, Li JF (2006) Normal sintering of (K, Na)NbO_3-based ceramics: Influence of sintering temperature on densification, microstructure, and electrical properties. J Am Ceram Soc 89:3669–3675

[44] Tsuji K, Ndayishimiye A, Lowum S, Floyd R, Wang K, Wetherington M, Maria J-P, Randall CA (2020) Single step densification of high permittivity $BaTiO_3$ ceramics at 300°C. J Eur Ceram Soc 40:1280–1284

[45] Guo H, Guo J, Baker A, Randall CA (2016) Hydrothermal-assisted cold sintering process: a new guidance for low-temperature ceramic sintering. ACS Appl Mater Interfaces 8:20909–20915